Bulgarian Journal of Physics vol. **50** (2023) 398–411

R/S Analysis on Multiparticle Production Process in Nucleus–Nucleus Collisions at Different SPS Energies

Nirpat Subba[1], **Azharuddin Ahmed**[1], **Abdel Nasser Tawfik**[2], **Prabir Kumar Haldar**[1*]

[1]Department of Physics, Cooch Behar Panchanan Barma University, Vivekananda Street, Cooch Behar - 736101, India
[2]Future University in Egypt (FUE), Fifth Settlement, End of 90th Street, New Cairo - 11835, Egypt
[*]Corresponding author's E-mail: prabirkrhaldar@gmail.com

Received: 18th of May 2023
doi: https://doi.org/10.55318/bgjp.2023.50.4.398

Abstract. The rescaled range analysis technique has been implemented to investigate the multiparticle production dynamics of ^{16}O-Ag/Br interactions at 60A GeV and ^{32}S-Ag/Br interactions at 200A GeV. We have analyzed the properties like multifractality, scale-freeness, and correlation among the produced particles. We have also used the simulated event generators UrQMD and AMPT model to compare with the experimental data sets. It has been observed that for ^{16}O-Ag/Br interactions, the AMPT simulated data shows more consistency compared to both experimental and UrQMD simulated data. Similarly for ^{32}S-Ag/Br interactions, the experimental data set shows more long-term positive autocorrelation in comparison with AMPT and UrQMD simulated data sets. It has been also observed that the rescaled range analysis technique is very prominent to describe the multiparticle production dynamics in relativistic heavy ion collisions.

KEY WORDS: R/S analysis, Multifractality, Correlation, Heavy-ion collisions

1 Introduction

Over the last few decades, the relativistic heavy ion collisions have made a huge impact on the field of Quark Gluon Plasma (QGP). A notable number of leading researchers have been investigating the existence of QGP [1–5]. In this regard, a significant number of heavy ion experiments have been performed, at different international reputed laboratories, like Relativistic Heavy Ion Collider (RHIC) at BNL and the Large Hadron Collider (LHC) at CERN [6–9]. Different targets and projectiles are used at different energies ranging from SPS to LHC. Many studies have been performed for deep understanding of the multiparticle production process by using different analytical tools [10–16]. It is worthwhile to

mention that the scale invariance or self-similarity analogous to that often encountered in complex non-linear systems leading towards deeper insight in long distance of regime of Quantum Chromodynamics (QCD) and unsolved problem of colour confinement.

Over the last few years, a major shift has been taken out in the field of heavy ion collisions with the help of complex network analysis. Albert and Barabasi had studied this field for the first time [17, 18] and examined some analytical techniques for the scale-free networks. After that Lacasa *et al.* [19] proposed a method to study the time series into a network. Apart from these, there are lots of interesting methods that have been developed to study the fractality and long-range dependencies of a time series [20, 21]. The term *"fractal"* was first used by Mandelbrot in his book *"The Fractal Geometry of Nature"* [22].

The fractal patterns can be characterized using an index, fractal dimension D. Such fractal dimension has its tremendous application in several fields, including medicine [23, 24], human physiology [25], etc. Such an idea was first implemented in mathematics by Benoit Mandelbrot in 1977 [26]. In the year 1979, it was observed in quantum mechanics, the path of a particle represents a fractal curve and such nature indicates the Heisenberg uncertainty principle [27]. Moreover, such paths followed self-similarity patterns under certain circumstances that represent most fractals' properties. One can say that such paths are complicated to be studied under ordinary space and require something more to be well defined. As such fractal dimension, D is being introduced, which can also gather information about the experimental data. Fractals are things with a non-integral dimension that are self-similar. The fractal dimension is a non-integer generalisation of regular topological dimensionality. There are more complex self-similar objects, which are made up of differently weighted fractals with varying non-integer dimensions. It is known as multifractals and are defined by generalized dimensions $D(q)$ which depend on the rank q of the moment of the probability distribution over such objects. [15].

So considering self-similar time series, the fractal dimension D can be related with the Hurst exponent as $D = 2 - H$, where D lies between 1 and 2 in one-dimension. The Hurst exponent measures the long-term memory in time series and it's value varies between 0 and 1. Such Hurst exponent gives the measurement of the smoothness in the fractal objects. The value of the Hurst exponent in the range > 0.5 denotes persistent, whereas < 0.5 indicates antipersistent. Hence, one can say that the higher values of such exponent represent more smoothness and less volatility.

The information on correlation and persistence can also be well explained by the Hurst exponent, making it an exceptional tool for analyzing the fractal nature. Further, it was signaled out that H can be analyzed using rescaled range (R/S) analysis, which measures the statistical variability of the time series. The purpose of such analysis is to identify how the apparent variability of a series

changes with the considered time period. In this study, we have used the experimental data from $^{16}O - Ag/Br$ interactions at energy 60A GeV and ^{32}S-Ag/Br interactions at 200A GeV. We have also compared the experimental results with the UrQMD and AMPT simulated event samples.

The manuscript is prepared as follows: In Section 2, we have mentioned the goal of the present study. In Section 3, we have described the data analysis, which includes experimental details, UrQMD model and AMPT model. Section 4 bears the detailed study about the method applied in this work. In Section 5, we have presented our results and discussions from this study. Section 6 includes the conclusions of the present work. At last, we have narrated the acknowledgments section, followed by the conflict of interest.

2 Goal of the Study

There are many studies performed to investigate the multifractality of the multiparticle production process in high energy heavy ion collisions. In the recent past, a notable number of researchers have conducted many complex network analysis techniques like visibility graph (VG), horizontal visibility graph (HVG), and Sandbox algorithm (SB) on different data-sets [28–31]. Different studies show some remarkable findings of the multiparticle production processes. But to date, there is no such study of the multiparticle production process using the R/S analysis method has been performed. So, in this work, we have performed the multifractality, scale freeness and correlations among the produced particles in the light of rescaled range analysis method. For the study purpose, we have considered data sets of ^{32}S-Ag/Br interactions at 200A GeV and ^{16}O-Ag/Br interactions at 60A GeV. We have also used the UrQMD and AMPT simulated data to compare with the experimental results.

3 Data Analysis

3.1 Experimental details

The experimental data applied to this study have been extracted from the photo emulsion plate exposed ^{16}O beam, at energy 60A GeV and ^{32}S beam, at 200A GeV, at SPS at CERN. More details about the experimental data sets can be found in ref. [32–34]. In this section, we focus on the selection of the events from the respective interactions.

A total number of 250 Ag/Br events of 60A GeV ^{16}O induced interactions and 140 Ag/Br events of 200A GeV ^{32}S induced interactions are chosen for the analysis based on the above selection criteria. Here, the nuclear emulsion plates have been considered as targets and as the detector, as well. Now, as per the condition of the nuclear emulsion terminology [35] all charged particles of the events are

identified by gray, black and shower particles. The particles produced in relativistic heavy ion collisions having ionization density $I < 1.4I$ and velocity $v \geq 0.7c$ are termed as shower particles. These shower particles are basically known as pions.

3.2 UrQMD model

One of the most important simulated event generators in high-energy heavy ion collisions is Ultrarelativistic Quantum Molecular Dynamics (UrQMD) [36–38], which has been employed to compare with the experimental results of nucleus–nucleus collisions. UrQMD is a microscopic transport model relying on covariant propagation of hadrons along classical path conjunction with colour string generation, binary scattering, and resonance decay [39]. UrQMD is a Monte Carlo (MC) solution to a huge collection of the linked partial equation that involves both derivatives and integrals of a function for the temporal evolution of various phase-space densities. Its primary components are two body potentials, resonance decay width, and binary reaction's cross-section. It contains 55 species of baryons, including delta particles, nucleon, and hyperon resonance. It also explains very well 32 meson species, isospin of all hadrons, and the symmetry of baryons and antibaryons [40]. The applicable energy range of this model varies between $E_{\text{lab}} = 100$ MeV/nucleon to $E_{\text{lab}} > 200$ GeV/nucleon. At lower energies, nucleus–nucleus collisions in UrQMD simulations may be described by hadronic degrees-of-freedom [41]. An important parameter associated with this simulation method is *"impact parameter"*, which is denoted by b, and the condition of this parameter should be $b < \sqrt{\sigma_{\text{tot}}}/\pi$, where σ_{tot} is the total cross-section. It is noted that the quark–hadron phase transition and quark gluon plasma are not included in this model. The intermediate fireball of the thermal and chemical equilibrium environments can be well described by this model. However, more details about the RQMD and UrQMD model can be found in ref. [34, 42, 43].

3.3 AMPT model

Since the UrQMD model is not sufficient to fully describe the multiparticle production dynamics, hence we have used another simulated event generator called A Multi Phase Transport (AMPT) [44–46] model to compare the experimental as well as UrQMD, simulated data [47]. In relativistic heavy ion collisions, AMPT is nothing but a Monte Carlo event generator. For the generation of initial conditions, HIJING (Heavy-Ion Jet Interaction Generator) model [48] has been used as an input. The initial conditions for the default version are minijets, string, and Lund model. The string formation is based on the Lund model as the case in HIJING. The string–liquifying version of AMPT handles the primary condition of partons and describes hadronization using the simple coalescence model. The main concept of the HIJING model is that any nucleus–nucleus collisions can

be treated as the superposition of many binary nucleon–nucleon collisions in association with the impact parameter. In that case Wood–Saxon distribution has been implemented to generate and calculate the value of the impact parameter. Then, the eikonal formalism is used to determine the probability of a collision to occur. For a particular collision, it can be determined whether it is an elastic or inelastic interactions. The nuclear effects in inelastic hard collisions are considered and taken into account by employing the parton distribution function associated with the impact parameter. Such distribution function is evaluated based on the Mueller–Qiu [49] parameterization of the nuclear shadowing. Furthermore, to describe the hard collision, PYTHIA routines [50] are utilized, whereas the Lund model dictates for soft collisions [51]. Further details about the AMPT model can be found in [44–46].It is also worth mentioning that the AMPT model can be treated as an important source describing many underlying dynamics of the multiparticle production process [52–54]. The existence of clusterization and correlation among the produced particles can also be produced by this model.

For the present study, the UrQMD code (version 3.4) and the AMPT model (ampt-v1.21-v2.21.tgz) are utilized in their default setting to generate the events in η-space for both ^{16}O-Ag/Br interaction at 60A GeV and ^{32}S-Ag/Br interaction at 200A GeV. To generate the minimum bias event samples in the laboratory frame, events are generated for the Ag and Br targets and ^{16}O and ^{32}S projectile nuclei at their respective incident energies separately. Maintaining the proportional abundances of these nuclei in G5 emulsion, the Ag and Br events are mixed up for each projectile and the minimum biased sample is obtained. From these samples, a subsample is selected that matches the respective experimental multiplicity and pseudorapidity distributions. The obtained final sample of simulated events for each projectile is five times as large as the corresponding experiment (as mentioned earlier, we have taken 250 experimental events for ^{16}O-Ag/Br interaction at 60A GeV and 140 experimental events for ^{32}S-Ag/Br interaction at 200A GeV). In this present work, we have used these model to compare the results from experimental data sets.

4 Rescaled Range Analysis Method

The R/S method of analysis is the oldest and best known method for the complex network analysis, which was introduced by Arold Edwin H. Hurst [55] and is popularized by Wallis and Mandelbrot [56–58], is discussed in detail. Here, we give a brief description of R/S methods [55–59]. The R/S statistics usually deals with the range of partial sums of deviations of sequences in a data (*or time*) series from its mean, which is rescaled by the standard deviation. The whole statistics can be summed up in five steps given below,

1. Consider a data series with N number of nodes (mass), where nodes are represented as $X_N = (x_i)$. From these nodes N, a subseries with M number of nodes is defined such as $Y_M = (y_j)$, where $M = sN$, and

$s \in (0,1)$.

2. Then for this subseries, a mean is computed by using relation

$$\bar{y_s} = \frac{1}{M}\sum_{k=1}^{M} y_k \,. \tag{1}$$

3. Create a cumulative data series of the partial summations

$$z_i = \sum_{k=1}^{i} y_k \sim \bar{y_s} \quad \text{where} \quad i = 1, 2, \ldots, M \,. \tag{2}$$

4. The range can then be obtained

$$R_s = {}_{\max}\, z_i - {}_{\min} z_i \,. \tag{3}$$

5. The range is rescaled by the standard deviation σ_s,

$$(R/S)_s = \frac{R_s}{\sigma_s} \,, \tag{4}$$

where the sample standard deviation σ_s is given by

$$\sigma_s = \Big[\frac{1}{M}\sum_{k=1}^{M}(y_k \sim \bar{y_s})^2\Big]^{\frac{1}{2}} \,. \tag{5}$$

These steps can be summarized in a single equation as

$$(R/S)_s = \frac{1}{\sigma_s}\left[\max\Big(\sum_{k=1}^{i}(y_k - \bar{y_s})\Big)_{1\le i\le M} - \min\Big(\sum_{k=1}^{i}(y_k - \bar{y_s})\Big)_{1\le i\le M}\right]. \tag{6}$$

It is evident that $(R/S)_s$ gives the maximum possible distance that one can walk with step Y_M. For a given s, the rescaled range is estimated for a large number of random subsample and then averaged over the whole fractal domain N. Similar calculations are performed with different values of s. If the data series X_N is stochastic process then over a domain ($s \in (s_{\min}, s_{\max})$, the R/S statistics obeys a power law,

$$(R/S)_s \propto s^H \,, \tag{7}$$

where H is the Hurst scaling exponent. Thus, a log–log plot of $(R/S)_s$ as a function of the scale s [$s \in (s_{\min}, s_{\max})$] gives a straight line with slope H.

The (R/S) analysis is then generalized in the norm of q for multifractal estimation of generalized Hurst exponent H_q.

$$\sigma_{s,q} = \Big[\frac{1}{M}\sum_{k=1}^{M}(y_k - y_s)^{1/q}\Big]^q \,. \tag{8}$$

As above, one can expect R/S statistics to obey a power law,

$$(R/S)_{s,q} = a_q s^{H_q} . \tag{9}$$

In this multifractal analysis, higher values of q boost the larger fluctuations $y_k - y_s$ from the mean y_s. Similarly, lower values $q \to 0$ provides an equal weight to large and small fluctuations from the mean. If the R/S method for multifractal system results in a constant H_q for all $q \in R$, then the data series X_N is monofractal in nature. This means that the data series is a construct of only one fractal generator.

However, if the generalized Hurst exponent H_q isn't constant and varies over a domain $0 \leq H_q \leq 1$, the data series is complex and multifractal. This means that the data series may be more complex compared to the monofractal system since it is a construct of more than one fractal generator. H_q plays an important role in the description of the smoothness of the data series. It assesses the relative propensity of a data series. For $H_q = 0.5$, the data series belongs to a random process with no correlations. On the other hand, if $H_q < 0.5$, the correlations in the data series are antipersistent in nature, where higher values are likely to be followed by lower values. If $H_q > 0.5$, the correlations in the data series are persistent in nature, where higher or lower values are likely to be followed by the same types of values. The R/S method traces the n-dimensional data (*or time*) series pointwise, that forms a curve in $(n+1)$-dimension [59, 60]. Thus, the generalized Hurst exponent H_q is related to the multifractal dimension D_q in n-dimension by the relationship,

$$D_q = n + 1 - H_q . \tag{10}$$

Since, the generalized Hurst exponent H_q lies in the domain $0 \leq H_q \leq 1$, the multifractal dimension D_q varies between $1 \leq D_q \leq 2$ in 1-dimension.

5 Result and Discussions

To explore the fractal behaviour of multiparticle production process, rescaled range method is implemented on the experimental data of ^{16}O-Ag/Br interactions at 60A GeV and ^{32}S-Ag/Br interactions at 200A GeV, SPS energies. Their corresponding AMPT and UrQMD simulated data are also being used to investigate and compare with the experimental data sets. Here, the rescaled range has been estimated over many random subsample with different scales s varying between 0.06 and 0.5 with an interval of 0.01.

It is worth highlighting that for scale $s_{\min} < 0.06$, the finite size effect will result in overestimating the Hurst exponent and is not considered. A similar effect occurs with scale $s_{\max} > 0.5$, which is mainly due to the small number of subsample, which fails to stabilize the rescaled range statistics. In this analysis, only those events are considered, which is a result of the head-on collisions, because

of their high multiplicity relative to other peripheral collisions. A collection of such events are taken, and their average multiplicity are calculated. Those events with multiplicity greater than the average multiplicity are taken for investigation using rescaled range method.

In this analysis, the rescaled range $(R/S)_{q,s}$ are obtained for different scale s for a given q-norm of a random subsample for an event. It is then averaged over a subsample in that event. Similar calculations are carried out for different events and are again averaged for all number of events (N_{event}). The error associated with the event averaged rescaled range $\langle(R/S)_{q,s}\rangle$ are then calculated from the standard deviation of the rescaled range $(R/S)_{q,s}$ of each event from the event averaged rescaled range $\langle(R/S)_{q,s}\rangle$. i.e.,

$$\sigma(\langle(R/S)_{q,s}\rangle) = \sqrt{\frac{\sum_{i=1}^{N_{\text{event}}}\left[\langle(R/S)_{q,s}\rangle - (R/S)_{q,s}\right]^2}{N_{event}-1}}, \tag{11}$$

where $\langle\cdots\rangle$ represents the average over the total number of events.

The logarithm of rescaled range $\ln(R/S)_{q,s}$ are then plotted against $\ln(s)$. Figures 1 and 2 show the variation of $\ln(R/S)_{q,s}$ and $\ln(s)$ with error bars for $q = 1, 2, 4, 6, 8, 10$ and 12. In this case, 20 independent samples of UrQMD and AMPT have been generated using different seeds and are entirely independent of one another. The errors are derived from the statistical dispersion of the mean value of the quantities from each sample.

$$\sigma(\overline{\langle(R/S)_{q,s}\rangle}) = \sqrt{\frac{\sum_{i=1}^{N_{\text{sample}}}\left[\overline{\langle(R/S)_{q,s}\rangle} - \langle(R/S)_{q,s}\rangle_i\right]^2}{N_{\text{sample}}-1}}, \tag{12}$$

where $\overline{X}$ represents the average over 20 independent sample sets (X being the placeholder of quantity under study). The uncertainties shown in Figures 1 and 2 are merely statistical. These uncertainties mainly depend on the data dispersion of the mean value. Furthermore, another important uncertainty factor is the number of data available, i.e., the more data points, the more adequate observations can be made. Besides statistical uncertainties, systematic uncertainties may also occur [34]. The $\ln(R/S)_{q,s}$ are found to be linear dependent of $\ln(s)$ with slope given by $H(q)$ called q^{th} scaling exponent.

From the plot of q, no distinct crossover region is observed for both $^{16}O - Ag/Br$ and $^{32}S - Ag/Br$ interactions. Thus, the multiparticle production process is a scale independent process meaning the correlation exists the same throughout the rapidity space irrespective of its scale measurement. The same is also reported in our previous paper using different method [29]. If anyway, the process has been scale dependent, then the above graph would have a crossover region, where the two different lines with different slopes meet, due to which it would not be uniquely defined by a power law. The generalized Hurst exponent

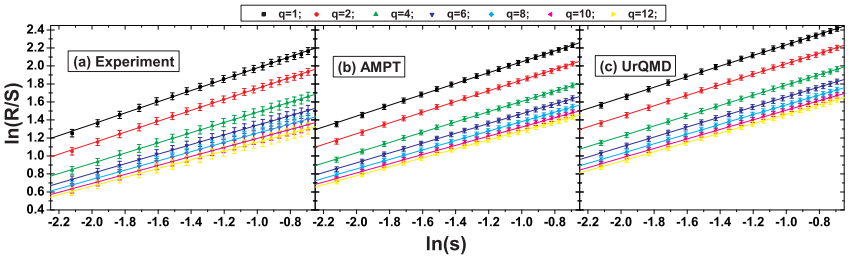

Figure 1. Variation of the logarithm of rescaled range $(\ln(R/S))$ with $\ln(s)$ for ^{16}O-Ag/Br interactions at 60A GeV.

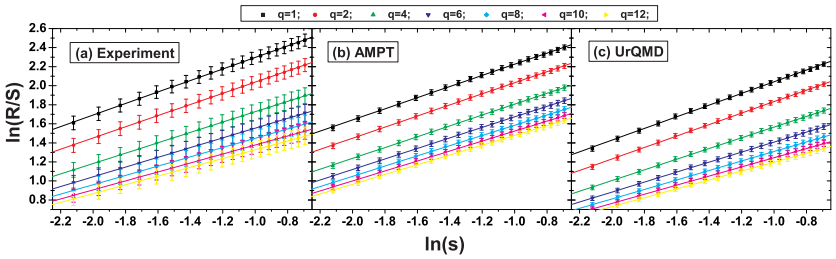

Figure 2. Variation of the logarithm of rescaled range $(\ln(R/S))$ with $\ln(s)$ for ^{32}S-Ag/Br interactions at 200A GeV.

$H(q)$ is then obtained for different values of scale factor q from linear regression performed on $ln(R/S)_{q,s}$ and $\ln(s)$. The variation of generalized Hurst exponent $H(q)$ and q are shown in Figure 3.

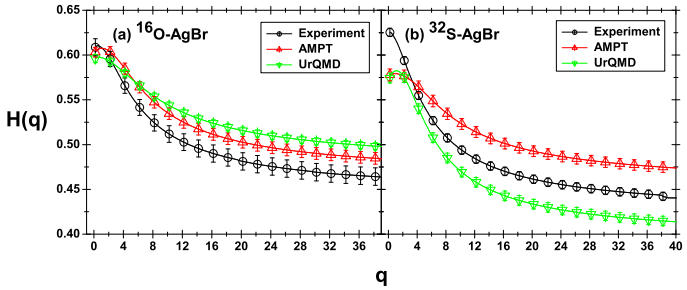

Figure 3. Variation of the Hurst exponent $H(q)$ with scale factor q.

From the graph, it is evident that the experimental data sets for both ^{16}O-Ag/Br and ^{32}S-Ag/Br interactions are more multifractal compared to AMPT and UrQMD simulated data sets. The range of generalized Hurst exponent for ^{16}O-Ag/Br varies between $0.45 - 0.61$ and for ^{32}S-Ag/Br between $0.4 - 0.63$. The values of H_q for both ^{16}O-Ag/Br and ^{32}S-Ag/Br interaction are less than unity,

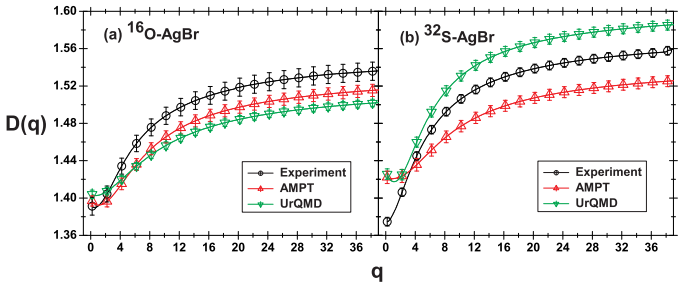

Figure 4. Variation of the fractal dimension $D(q)$ with scale factor q.

this signals that the multiparticle production process is the self-affine process and is anisotropic in nature. If the process is isotropic and self-similar, then the value of H_q would be unity. The generalized fractal dimension $D(q)$ is related to the generalized Hurst exponent as $D(q) = 2 - H(q)$ in one dimension. The variation of $D(q)$ with q is plotted in Figure 4.

For $q = 2$, the generalized Hurst exponent $H(q)$ is identical to H. Its corresponding fractal dimension $D(q)$ is identical to Hausdorff dimension which signify the roughness present in the said process. The corresponding values for Hurst exponent and Hausdorff dimension along with the degree of multifractality is listed in Table 1 and Table 2.

It is found from the data extracted so far, that for ^{16}O-Ag/Br interactions, the AMPT simulated data is slightly more persistent compared to the experimental data followed by UrQMD simulated data, however there are no significant differences observed.

Table 1. Hurst exponent H, Hausdorff dimension D and degree of multifractality ω for ^{16}O-Ag/Br interactions

Data type	$H(2)$	$D(2)$	ω
Experiment	0.598±0.008	1.402±0.008	0.16±0.014
AMPT	0.605±0.006	1.395±0.006	0.132±0.009
UrQMD	0.594±0.004	1.406±0.004	0.106±0.006

Table 2. Hurst exponent H, Hausdorff dimension D and degree of multifractality ω for ^{32}S-Ag/Br interactions

Data type	$H(2)$	$D(2)$	ω
Experiment	0.598± 0.004	1.402 ±0.004	0.229±0.006
AMPT	0.577±0.007	1.423±0.007	0.113±0.009
UrQMD	0.577±0.005	1.423±0.005	0.168±0.008

Similarly, for the ^{32}S-Ag/Br interactions, the experimental data set shows a more long-term positive autocorrelation in comparison with the AMPT and UrQMD simulated data sets, where the Hurst exponent obtained from AMPT and UrQMD is almost the same. However, it is globally observed that all the said interactions persist long-term positive auto correlations. Furthermore, the degree of multifractality, ω, is computed using equation $\omega = D_{\max} - D_{\min}$ and is listed in Table 1 and Table 2. It is observed that the experimental data sets are more multifractal compared to the both AMPT and UrQMD simulated data sets. In the case of experimental and UrQMD simulated data set, the degree of multifractality is seen more for ^{32}S-Ag/Br interactions compared to ^{16}O-Ag/Br. The same is not true for the AMPT simulated data sets. Also, for the ^{16}O-Ag/Br interactions, the AMPT is comparatively more multifractal compared to UrQMD data set, whereas for the ^{32}S-Ag/Br interactions, AMPT shows less fractality compared to UrQMD data set.

It is worthwhile to mention that the values of Hurst exponents H as well as Hausdorff dimensions D for the experimental data sets of both ^{16}O-Ag/Br interactions at 60A GeV and ^{32}S-Ag/Br interactions at 200A GeV are almost identical within errors. According to Mills proposal [61], the data set from two different projectile with different energies having the identical values of fractal dimension may indicate the common source. It may originate from a particular route i.e. QGP. It is further interesting to note that the degree of multifractality ω are found to be different for both the interactions where the value of ω for ^{32}S-Ag/Br interactions is greater than that of ^{16}O-Ag/Br interactions.

6 Discussions on Systematic Uncertainty

The uncertainty depicted in the graphs is solely statistical. In addition to analysing the influence of statistical uncertainty on our study, we must also assess the effect of systematic uncertainty. During the scanning and measuring processes in the nuclear emulsion detector, these systematic uncertainty may occur. A track scanning technology was used to find out about each interaction. The purpose of the "along the track" scanning approach is to collect precise event samples. It has already been stated that the study would exclude interactions occurring within $20\mu m$ of the top or bottom glass surface. Eliminating such events minimises track losses and systematic uncertainty. In order to increase scanning efficiency by up to 99%, we have created a system in which two observers monitor each event concurrently. This technique reduces counting, measurement and detecting inconsistencies. So, the measurement and scanning method contributes less than one percent to the systematic error. Details about the systematic uncertainty can be found in ref. [62].

7 Conclusions

In this present study, the multifractality, scale freeness, and correlation among the produced particles are performed for experimental as well as simulated data of $^{16}O - Ag/Br$ interactions at 60 AGeV and $^{32}S - Ag/Br$ interactions at 200 AGeV in the framework of rescaled range analysis method.

The important conclusions can be summarized as follows –

1. It has been observed that the multiparticle production process for ^{16}O-Ag/Br interactions at $60A$ GeV and ^{32}S-Ag/Br interactions at $200A$ GeV are scale free. This implies the existence of correlations among the produced particles throughout the pseudorapidity (η) space.
2. The generalized Hurst exponent $H(q)$ is calculated by using the values of scale factor q and the variation of $H(q)$ and q as plotted in Figure 3. The conclusion comes from Figure 3 that the experimental data for both types of interactions are multifractal in nature compared to the UrQMD and AMPT simulated data. It has also been observed that the values of $H(q)$ for both ^{16}O-Ag/Br and ^{32}S-Ag/Br interactions are less than one which indicates about the self-affinity of the multiparticle production process.
3. For both types of interactions, the experimental data shows more positive autocorrelation compared to UrQMD and AMPT simulated data sets.
4. The higher degree of multifractality ω in case of ^{32}S-Ag/Br interactions at $200A$ GeV may indicate the presence of more chaoticity in nature compared to ^{16}O-Ag/Br interactions at $60A$ GeV.
5. Fractal is a consequence of the QCD cascade within multiparticle production dynamics. Higher values of the fractal dimensions can indicate a type of possible phase transition during the multiparticle production process, e.g. equivalency of the higher order codimensions to the second order one. the monofractality (constant $D(q)$) is associated with thermal (second-order) phase transition. Consequently, monofractal behavior might be a signal for a quark–gluon plasma second-order phase transition.

The multiparticle production dynamics is yet to come out with accurate parameters. The latest methodologies give more deterministic informations in terms of precise topological parameters to explore the dynamics of the multiparticle production process. Therefore, this is still an open area of research.

Acknowledgements

The authors heartily acknowledge Prof. D. Ghosh of Deepa Ghosh research foundation for all kind to supports and encouragements. One of the authors (A. Ahmed) acknowledges the state government fellowship scheme, Govt. of West Bengal, India. AT acknowledges the support offered by the Future University in Egypt (FUE)!

Conflict of Interest

The authors announce that they have no conflict of interest.

References

[1] P. Braun-Munzinger, J. Stachel (2007) *Nature* **448** 302-309.
[2] J.W. Harris, B. Müller (1996) *Annu. Rev. Nucl. Part. Sci.* **46** 71-107.
[3] B. Mueller (1985) *The Physics of the Quark-Gluon Plasma: Lecture Notes in Physics* **225** ISBN 978-3-540-15211-8. Springer-Verlag.
[4] D. Ghosh, et al. (2004) **65(4)** 472.
[5] A.M. Tawfik, E. Ganssauge (2000) Acta Phys. Hung. A **12** 53.
[6] J. Stachel, G.R. Young (1992) *Annu. Rev. Nucl. Part. Sci.* **42** 537-597.
[7] A. Tawfik (2011) *Nucl. Phys. A* **859(1)** 63-72.
[8] A. Tawfik, E. Gamal, A.G. Shalaby (2015) *Int. J. Mod. Phys. A* **30** 1550131.
[9] A. Accardi, et al. (2016) *Eur. Phys. J. A* **52(9)** 1-100.
[10] P.K. Haldar. et al. (2013) *Astropart. Phys.* **42** 76-85.
[11] P. Carruthers, I. Sarcevic (1989) *Phys. Rev. Lett.* **63** 1562.
[12] M. Szuba (NA49 Collaboration) (2011) *Indian J. Phys.* **85** 1057.
[13] K. Redlich, F. Karsch, A. Tawfik (2004) *J. Phys. G: Nucl. Part. Phys.* **30(8)** S1271.
[14] A. Tawfik (2013) *Phys. Rev. C* **88** 035203.
[15] E.A. De Wolf, I.M. Dremin, W. Kittel (1996) *Phys. Rep.* **270(1-2)** 1-141.
[16] A. Tawfik (2014) *SOP Trans. Theor. Phys.* **1** 7-13.
[17] R. Albert, A.L. Barabasi (2002) *Rev. Mod. Phys.* **74** 47-97.
[18] A.L. Barabasi (2011) *Nat. Phys.* **8** 4-16.
[19] L. Lacasa *et al.* (2008) *Proc. Natl. Acad. Sci. USA* **105** 4972.
[20] T. Tél, Á. Fülöp, T. Vicsek (1989) *Physica A* **159** 155-166.
[21] W. Kittel, E.A. De Wolf (2005) "*Soft multihadron dynamics*", World Scientific.
[22] B.B. Mandelbrot (1983) "*The Fractal Geometry of Nature*", Freeman.
[23] D.P. Popescu, et al. (2010) *Biomed. Opt. Express* **1(1)** 268-277.
[24] R.D. King *et al.* (2009) *Brain Imaging and Behavior* **3(2)** 154-166.
[25] Y. Chen (2011) *PLOS ONE* **6**(9) e24791.
[26] B. Mandelbrot (1977) "*Fractal form, chance and dimension*". San Francisco, Freeman.
[27] L.F. Abbott, M.B. Wise (1981) *Am. J. Phys.* **49(1)** 37-38.
[28] A. Ahmed, et al. (2021) *Eur. Phys. J. Plus* **136** 100.
[29] N. Subba, et al. (2021) *Int. J. Mod. Phys. E* **30(1)** 2150002.
[30] P. Mali, et al. (2018) *Physica A: Stat. Mech. Appl.* **493** 253-266.
[31] P. Mali, A. Mukhopadhyay, S.K. Manna, P.K. Haldar, G. Singh (2017) *Mod. Phys. Lett. A* **32** 1750024.
[32] D. Ghosh, et al. (1995) *Phys. Rev. C* **52** 2092.
[33] D. Ghosh, et al. (1999) *Europhys. Lett.* **48** 508.
[34] A. Ahmed, et al. (2021) *Eur. Phys. J. A* **57** 322.

[35] C.F. Powell, P.H. Fowler, D.H. Perkin (1959) "*The Study of the Elementary Particles by Photographic Method. An Account of the Principal Techniques and Discoveries Illustrated by an Atlas of Photomicrographs*". Pergamon Press, Oxford, pp. 450-464.
[36] M. Bleicher, et al. (1999) *J. Phys. G* **25** 1859.
[37] S.A. Bass, et al. (1998) *Prog. Part. Nucl. Phys.* **41** 255.
[38] M. Bleicher, et al. (1998) *Phys. Lett. B* **435**(1-2) 9-12.
[39] M. Bleicher, S. Jeon, V. Koch (2000) *Phys. Rev. C* **62**(6) 061902.
[40] Z. Lin, C.M. Ko (2001) *Phys. Rev. C* **64**(4) 041901.
[41] M. Bleicher, et al. (1998) *Nucl. Phys. A* **638**(1-2) 391-394.
[42] P. Mali, S.K. Manna, P.K. Haldar, A. Mukhopadhyay, G. Singh (2017) *Chaos, Solitons & Fractals* **94** 86-94.
[43] Z. You, W. Ke-Jun, L. Feng (2010) *Chinese Phys. C* **34**(9) 1436.
[44] B. Zhang, C.M. Ko, B.A. Li, Z.-Wei Lin (2000) *Phys. Rev. C* **61** 067901.
[45] Z.W. Lin, et al. (2001) *Phys. Rev. C* **64** 011902.
[46] Z.W. Lin, et al. (2005) *Phys. Rev. C* **72** 064901.
[47] B. Ali, S. Singh, S. Ahmad (2022) *Eur. Phys. J. Plus* **137**(2) 1-18.
[48] X.N. Wang, M. Gyulassy (1991) *Phys. Rev. D* **44** 3501.
[49] A.H. Mueller, J. Qiu (1986) *Nucl. Phys. B* **268** 427.
[50] T. Sjostrand, S. Mrenna, P. Skands (2006) *JHEP* **0605** 026.
[51] B. Andersson, G. Gustafson, B. Nilsson-Almqvist (1987) *Nucl. Phys. B* **281** 289.
[52] PHOBOS Collaboration (P. Steinberg, et al.) (2006) *Nucl. Phys. A* **774** 631.
[53] B.B. Back, et al. (2006) *Phys. Rev. C* **74** 011901 .
[54] N. Li, et al. (2012) *J. Phys. G: Nucl. Part. Phys.* **39** 115105.
[55] H.E. Hurst (1951) *Trans. Am. Soc. Civ. Eng.* **116** 770.
[56] B.B. Mandelbrot, J.R. Wallis (1968) *Water Resour. Res.* **4**(5) 909-918.
[57] B.B. Mandelbrot, J.R. Wallis, R. James (1969) *Water Resour. Res.* **5**(5) 967-988.
[58] B.B. Mandelbrot, J.R. Wallis (1969) *Water Resour. Res.* **5** 228.
[59] J. Alvarez-Ramirez, J.C. Echeverria, E. Rodriguez (2008) *Physica A* **387** (26) 6452-6462.
[60] M. Bodruzzaman, et al. (1991) *IEEE Proceedings of the SOUTHEASTCON '91* **2** 1121-1123.
[61] S. Mills (1990) The application of fractal dimensional analysis to high energy physics events. *No. CERN-ALEPH-NOTE-90-003*.
[62] S. Bhattacharyya (2021) *Eur. Phys. J. A* **57** 164.